Analysis of post-derailment dynamic behaviour of a railway vehicle and interaction with deformable containment structure

Matteo Santelia, Francesco Mazzeo, Egidio Di Gialleonardo, Stefano Melzi, Stefano Bruni

Department of Mechanical Engineering
Politecnico di Milano
Via La Masa, 1 I-20156 Milan, Italy
matteo.santelia@polimi.it

ABSTRACT

Nowadays, railway play an important role in land transportation, both of goods and passengers, and it is considered one of the safest means of transport. However, train derailments represent a relatively frequent cause of accidents and are likely to occur under different conditions: structural defects (both in tracks and running gears), bad quality of the infrastructure, problem occurring at wheel-rail interface, extreme weather, human error or impact with obstacles [1, 2]. Some experiments have been carried out to reproduce and analyse controlled derailments [3, 4], however it is extremely challenging and expensive to perform these typology of experiments. Thus, mathematical models and numerical simulations are adopted to study derailment events [5, 6]. The aim of this paper is to present a non-linear multibody model for simulations in time-domain of the post-derailment behaviour of railway vehicle and the subsequent interaction with a derailment containment structure. The vehicle is schematized as a set of rigid bodies connected through different linear and nonlinear visco-elastic components representing suspension elements. In addition to this, a wheel-rail contact model and a model of the track are introduced. Regarding the schematization of the containment structure, a finite element model (FEM) has been adopted and MATLAB was used as the environment for the realization of the simulation package.

Keywords: derailment, post-derailment dynamics, derailment containment structure, multibody

1 INTRODUCTION

Train derailments still remain nowadays a major problem in the rail transport sector. These events can lead to catastrophic consequences in terms of passenger safety and also to economic losses, damages to the structure surrounding the railway network and interruption of service. The increase in train service speed, especially in the high-speed sector, has led this problem to become more and more critical, especially with regards to passenger's safety. For this reason, railway industry has increasingly focused on understanding the causes of derailments, and on finding measures to avoid them [5, 7]. Active safety controllers have been introduced to reduce the number of derailment accidents due to improper operation mainly caused by over-speeding or high-speed train collisions. However, despite the use of advanced signalling and traffic control systems and the enhancement of vehicle reliability, derailments continue to occur due to various reasons which can be related to human error, poor infrastructure condition, mechanical failure, impact with obstacles or even earthquakes [1, 8, 9].

These safety-critical events can cause not only damage to the railway vehicle itself but also secondary damage to the surrounding infrastructure. In fact, there are high-risk zones along the railway network where the consequences of a train derailment can be catastrophic in terms of casualties and damages.These include, e.g., viaducts, stations entrances and areas where the railway track is very close to surrounding domestic or industrial buildings. For these reasons, various

passive measures have been studied, aimed to mitigate the outcome of a derailment. A solution presented in [10] is to attach guidance mechanisms to the bogie frame in order to constrain the lateral motion of the vehicle once it is derailed. Another possibility, proposed in [11], is to use geometrical specifications of the rolling stock component allowing the use of brake discs, gearboxes or bogie frames to obtain a similar effect. A final option is to adopt infrastructure-based devices: both guard-rails and containment walls have been studied. In [12] guard-rails placed between running rails are studied to prevent secondary damage caused by derailed trains on high-risk lines, whereas in [13, 14] the containment capacity and crash-worthiness of a derailment containment wall is evaluated using a finite element analysis to perform a collision simulation. Some experiments have been carried out to reproduce and analyse controlled derailments and different measures to mitigate them [3, 4]. However, it is extremely challenging and expensive to perform these typology of in-field tests. For these reasons, numerical simulations are mainly performed to study derailment events [9, 10]. In this paper a non-linear multibody model, for the simulation in time-domain of the post-derailment behaviour of railway vehicle and the subsequent interaction with a derailment containment wall is presented. The behaviour of the interaction of the containment structure with the derailed train is investigated using a finite element model (FEM), assembled with plate elements. In particular, in this paper, emphasis is placed on deriving estimates of the impact force applied by the derailed vehicle on the containment wall and on the resulting bending moment at the base of the wall. Finally, a sensitivity analysis on the effect of some parameters describing the position and dimension of the DCW is performed.

2 VEHICLE AND DERAILMENT CONTAINMENT WALL MODELS

The proposed 3D train model considers a single vehicle with one carbody, two bogies and four wheelsets, all considered as rigid bodies. Each rigid body has six degrees of freedom (DOF), resulting in a total of 42 DOF system. Each bogie is connected to two wheelsets by primary suspensions and to the carbody by secondary suspensions. The suspensions (both primary and secondary) are modelled by a set of massless visco-elastic elements with non-linear characteristics defined in the form of force-deformation or force-velocity curves. The equations of motion describing the system dynamics are expressed as:

$$\mathbf{M}(\mathbf{x})\ddot{\mathbf{x}} = \mathbf{Q_v}(\mathbf{x},\dot{\mathbf{x}}) + \mathbf{Q}(\mathbf{x},\dot{\mathbf{x}},t). \tag{1}$$

Where $\mathbf{x}$ is the vector collecting the 42 independent coordinates of the system, $\mathbf{M}(\mathbf{x})$ is the configuration dependent mass matrix of the vehicle, $\mathbf{Q_v}$ is the vector of generalized inertia forces which are a quadratic function of the vehicle's velocity $\dot{\mathbf{x}}$, and $\mathbf{Q}$ is the vector of the generalized forces acting on the vehicle. This latter term can be in turn expressed as the sum of the contribution of different forces acting on the system:

$$\mathbf{Q}(\mathbf{x},\dot{\mathbf{x}},t) = \mathbf{Q_g} + \mathbf{Q_s}(\mathbf{x},\dot{\mathbf{x}}) + \mathbf{Q_c}(\mathbf{x},\dot{\mathbf{x}},t). \tag{2}$$

Where $\mathbf{Q_g}$ is a constant vector defining the effect of weight on each body, $\mathbf{Q_s}$ the vector of generalised forces produced by suspension components and $\mathbf{Q_c}$ the vector of generalised forces arising from wheel-rail contact (or wheel-soil contact after derailment has occurred) at all wheels in the vehicle. The expressions of the mass matrix and of vectors $\mathbf{Q_v}$ and $\mathbf{Q_g}$ are derived according to standard multibody techniques as can be found in [15]. The derivation of vector $\mathbf{Q_s}$ for a generic suspension component is obtained using non-linear compact force element (CMP) models of suspension components [16], which allows to consider the stiffness or viscous damping properties along three directions defined in a component-specific reference system. Wheel-rail contact forces $\mathbf{Q_c}$ are introduced according to a simplified model, based on contact tables, in order to obtain a good trade-off between a fast and accurate estimation.

The vehicle model is finally coupled with a dynamic Finite Element Model (FEM) describing the behaviour of a deformable Derailment Containment Wall (DCW), as shown in Fig. 1. These two models interact through the exchanged forces once the derailed vehicle impacts against the structure. From a mathematical point of view, the system of equations describing the dynamics of the overall system composed by the vehicle and the derailment containment wall, is expressed as:

$$\begin{aligned} \mathbf{M}(\mathbf{x})\ddot{\mathbf{x}} &= \mathbf{Q_v}(\mathbf{x},\dot{\mathbf{x}}) + \mathbf{Q}(\mathbf{x},\dot{\mathbf{x}},t) + \mathbf{Q_{i,v}}(\mathbf{x},\dot{\mathbf{x}},\mathbf{x_s},\dot{\mathbf{x}}_\mathbf{s}), \\ \mathbf{M_s}\ddot{\mathbf{x}}_\mathbf{s} &= -\mathbf{K_s}\mathbf{x_s} - \mathbf{R_s}\dot{\mathbf{x}}_\mathbf{s} + \mathbf{Q_{i,s}}(\mathbf{x},\dot{\mathbf{x}},\mathbf{x_s},\dot{\mathbf{x}}_\mathbf{s}). \end{aligned} \tag{3}$$

Where the first system of equation represents the vehicle equations of motion (see Eq.s (1) and (2)), considering additionally the generalised forces on the vehicle coordinates caused by the impact with the DCW, whilst the second set of equations describes the dynamics of the DCW according to the FEM schematisation. The vector $\mathbf{x_s}$ collects the DOFs of the complete structure. Finally, as can be seen from Equations (3), the coupling terms of the two sets of equations are vectors $\mathbf{Q_{(i,v)}}$ representing the Lagrangian components of the impact forces respectively on the vehicle and on the deformable structure as nodal forces. Referring to second row in Equations (3), the terms $\mathbf{M_s}$,$\mathbf{R_s}$ and $\mathbf{K_s}$ represent respectively the mass, damping and the stiffness matrices of the complete FEM of the structure.

Equations (3) are used to estimate the impact forces and the bending moment in the DCW generated by the contact between parts of the rolling stock and the derailment containment structure built aside the track. The derailment scenario considered in this work was identified in agreement with experts from RFI (the Italian infrastructure manager) as particularly relevant to the structural sizing of the DCW and consists of the derailment of a high-speed vehicle travelling at 300 km/h in a curve with radius 5500 m and superelevation 95 mm. As can be seen from right drawing in Fig. 1 (left), the DCW (red line) is parallel to the track in the curve, and therefore its centre line in the horizontal plane is an arc of circumference with radius R_w. The curvature of the DCW is however neglected in the FEM model of the DCW, considering that the radius of the curve is two orders of magnitude larger than the length of the DCW interested by the impact with the vehicle. The portion of derailment containment wall modelled is 80 m long, 1.6 m tall and 0.3 m thick and is made of C30/37 reinforced concrete is used as construction material. Figure 1 (right) qualitatively shows the FEM model of the DCW, which is composed by 4-node rectangular Kirchoff plate elements. Each element has a length in longitudinal direction of 1 m and a height in vertical direction of 0.55 m, and the plate elements are arranged in three rows, resulting in 240 plate elements and 324 nodes of which 81, representing the foundations, are clamped. The expressions of the stiffness and mass matrices of each single plate element can be found in [17]. The structural matrices of the single elements are assembled to form the global structural matrices $\mathbf{M_s}$,$\mathbf{R_s}$ and $\mathbf{K_s}$ satisfying the conditions of equilibrium and congruence of displacements. In the FEM model of the DCW, the in-plane motion of the structure is neglected so the only generalised coordinates considered are z displacements, θ_x and θ_y rotation, according to the axes of the reference system shown in Fig. 1 (right). As far as the boundary condition are concerned, the nodes at the base of the DCW are fully constrained, to reflect the clamping of the lower base of the DCW.

The method adopted to compute the impact forces is based on the selection of suitable control points on the surface of the rolling stock, particularly the axle boxes and some points in the outer surface of the bogie frame. The trajectory of each control point is computed during the motion of the vehicle at each time-step in order to identify the positions at which contact with the containment structure occurs.

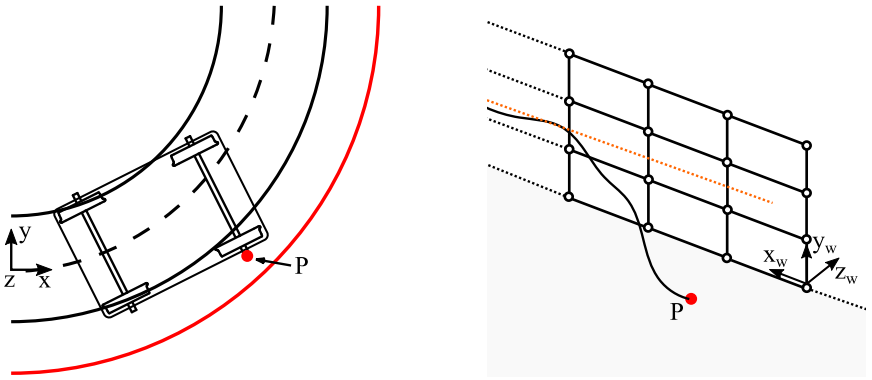

Figure 1: Left: Top-view of the front bogie and the derailment containment wall (in red) in the curved section. Right: 3-meter portion of FEM of the deformable structure. In both the sub-figures it is highlighted the potential contact point P.

For each i-th control point P_i, the distance from the undeformed DCW δ_i and its time-derivative $\dot{\delta}_i$ are computed as:

$$\begin{aligned} \delta_i &= \sqrt{(x_i - x_C)^2 + (y_i - y_C)^2} - R_w, \\ \dot{\delta}_i &= \dot{x}_i \frac{(x_i - x_c)}{\sqrt{(x_i - x_C)^2 + (y_i - y_C)^2}} + \dot{y}_i \frac{(y_i - y_C)}{\sqrt{(x_i - x_C)^2 + (y_i - y_C)^2}}. \end{aligned} \tag{4}$$

where subscript C denotes the coordinates of the curve centre (see Fig. (2)), subscript i denotes the coordinates of the i-th candidate contact point P_i, and R_w is the radius of the derailment containment structure. The initial impact is detected at point P_i when a positive value of the distance δ_i is found. From the point of initial contact, the curvilinear coordinate and vertical position of point P_i across the surface of the wall, s_i and h_i respectively, are computed as:

$$\begin{aligned} s_i &= R_w \alpha_i, \\ h_i &= z_i. \end{aligned} \tag{5}$$

where α_i is the angular position of point P_i with respect to the position of the initial contact and z_i is the vertical coordinate of the point in the absolute reference. In case multiple contact points between the vehicle and the wall occur at the same time, the angular position α_i of the different contact points are all referred to the position of the first impact, so that the relative position of the multiple contacts is preserved.

Finally the x_{wi} and y_{wi} coordinates of i-th control point in the $x_w - y_w - z_w$ reference system of the DCW FEM model (see Fig. (1) - right) are obtained as:

$$\begin{aligned} x_{wi} &= s_i + x_{w0}, \\ y_{wi} &= z_i - h_b. \end{aligned} \tag{6}$$

where x_{w0} is the initial distance of the impact point from one end of the FEM model and is set to 10 m (i.e. 12.5% of the total length of the model) to minimise the effect of the model's boundaries on the calculation of the deflection of the wall. In Eq. (6) h_b is the vertical position of the base of the DCW in the absolute reference.

Once the coordinates of the potential contact point are computed in the local reference frame of the containment structure using Equations (6), it is possible to find the single plate element in the FEM model being in contact with the vehicle at control point P_i. Next, the non-dimensional local coordinates ξ_i and η_i with respect of the local reference frame of the element are calculated.

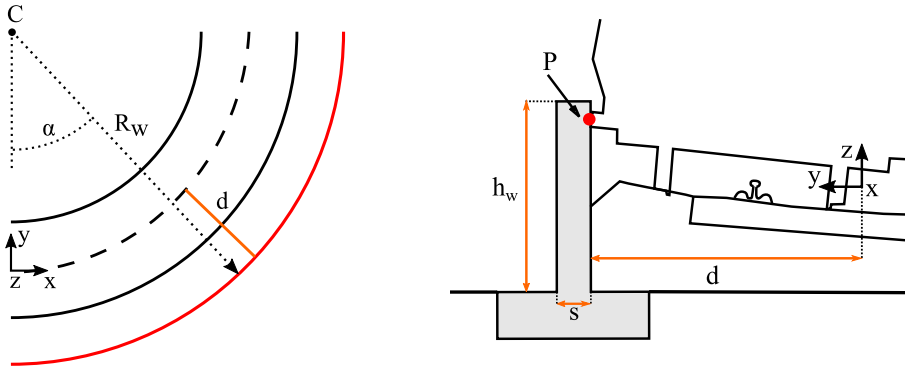

Figure 2: Left: Top-viev of the track layout (black lines) and DCW (red line). Right: Side-view of the DCW (in grey) with highlighted potential contact point P. With orange lines are reported the parameters defining the DCW.

Finally, the out-of-plane deflection w_i of the wall at the i-th contact point and its time-derivative $\dot{w}_i$ are obtained as:

$$\begin{aligned} w_i &= \phi_{\mathbf{i}}(\xi,\eta)^T \mathbf{x}_{\mathbf{s,i}}, \\ \dot{w}_i &= \phi_{\mathbf{i}}(\xi,\eta)^T \dot{\mathbf{x}}_{\mathbf{s,i}}. \end{aligned} \tag{7}$$

where ϕ_i is the vector of the shape functions of the plate finite element evaluated at the i-th contact point, $\mathbf{x_{s,i}}$ is the vector of nodal coordinates of the finite element obtained as $\mathbf{x_{s,i}} = \mathbf{E_i x_s}$, with $\mathbf{E_i}$ the Boolean extraction matrix selecting the coordinates of the impacted element in the vector$\mathbf{x_s}$ collecting all the nodal coordinates of the FEM model.

The normal component of the impact force at the i-th contact point is computed using the Lankarani-Nikravesh contact model [18], which allows to consider in an approximate way the local stiffness of the contacting bodies whilst the overall deformability of the DCW is modelled accurately thanks to the finite element model. The actual virtual compenetration $\overline{\delta}_i$ at the i-th contact point considering the deflection of the DCW and its time-derivative $\dot{\overline{\delta}}_i$ are obtained as:

$$\begin{aligned} \overline{\delta}_i &= \delta_i - w_i, \\ \dot{\overline{\delta}}_i &= \dot{\delta}_i - \dot{w}_i. \end{aligned} \tag{8}$$

The normal contact force is obtained, according to [18], as:

$$F_{N,i} = \begin{cases} H_c \bar{\delta}_i^{1.5} \left[1 + \frac{3(1-e^2)}{4} \frac{\dot{\bar{\delta}}_i}{\dot{\bar{\delta}}_i(-)} \right], & \bar{\delta}_i > 0 \\ 0 & \bar{\delta}_i \leq 0 \end{cases} \tag{9}$$

where H_c, is a Hertztian stiffness accounting for the local deformability of the structure and e is the coefficient of restitution which is related to local dissipative effects in the impact. A tangential force component is also considered to occur at the impact point, according to the law of dry friction. Using standard multibody techniques, the normal and tangential components of the impact forces at each active point of contact between the vehicle and the DCW are used to derive the vector $\mathbf{Q_{i,v}}$ of the generalised impact forces acting on the coordinates of the vehicle. Moreover, the normal force components $F_{N,i}$ are used to define the vector $\mathbf{Q_{i,s}}$ of the generalised nodal forces representing the effect of the impact on the FEM model of the DCW:

$$\mathbf{Q_{i,s}} = \sum_i \mathbf{E_i^T} \phi_{\mathbf{i}}(\xi_i,\eta_i) F_{N,i}. \tag{10}$$

The two coupled sets of equations 3 are numerically integrated in the time domain obtaining the motion of the vehicle and of the DCW, together with the time history of the impact force at all active impact points. As a post-processing of these results, the time history of the bending moment in the DCW is also obtained using the following equations [19]:

$$
\begin{aligned}
M_x(\xi,\eta) &= -D\left(\frac{\partial^2 w(\xi,\eta)}{\partial x^2}+\nu\frac{\partial^2 w(\xi,\eta)}{\partial y^2}\right) = -D\left(\frac{\partial^2 \phi_{\mathbf{k}}(\xi,\eta)^T}{\partial x^2}\mathbf{x}_{\mathbf{s},\mathbf{k}}+\nu\frac{\partial^2 \phi_{\mathbf{k}}(\xi,\eta)^T}{\partial y^2}\mathbf{x}_{\mathbf{s},\mathbf{k}}\right),\\
M_y(\xi,\eta) &= -D\left(\frac{\partial^2 w(\xi,\eta)}{\partial y^2}+\nu\frac{\partial^2 w(\xi,\eta)}{\partial x^2}\right) = -D\left(\frac{\partial^2 \phi_{\mathbf{k}}(\xi,\eta)^T}{\partial y^2}\mathbf{x}_{\mathbf{s},\mathbf{k}}+\nu\frac{\partial^2 \phi_{\mathbf{k}}(\xi,\eta)^T}{\partial y^2}\mathbf{x}_{\mathbf{s},\mathbf{k}}\right),\\
M_{xy}(\xi,\eta) &= (1-\nu)D\frac{\partial^2 w(\xi,\eta)}{\partial x\partial y} = (1-\nu)D\frac{\partial^2 \phi_{\mathbf{k}}(\xi,\eta)^T}{\partial x\partial y}\mathbf{x}_{\mathbf{s},\mathbf{k}}.
\end{aligned}
\tag{11}
$$

Where D is the flexural rigidity of the elementary plate element, defined as:

$$
D = \frac{Es^3}{12(1-\nu^2)}. \tag{12}
$$

where s is the thickness of the plate. Finally the integral of the bending moment is computed along the base of the derailment containment structure as:

$$
M_{tot} = \int_0^l M_y(\xi,\eta)dx. \tag{13}
$$

where l is the total length of the structure and M_y is the bending moment with respect of x_w axis in the local reference system as shown in Fig. (2).

3 SIMULATIONS AND RESULTS

To validate the vehicle model, simulations in 'standard' conditions where the vehicle has no mechanical problems and runs at a usual service speed through a curved section have been considered. The same vehicle and the same scenario have been modelled in software Simpack. For the sake of brevity the comparisons are not reported in these paper, but a very good agreement between the two models is observed and it can be concluded that the models of suspension components and of wheel-rail contact forces introduced ensure a good level of accuracy, at least as far as a standard running condition of the vehicle is considered. Next, the developed multibody/FEM model is applied to the case of a high-speed ETR-500 class locomotive running at 300 km/h along a curve with radius 5500 m and potential contact points are placed on the axle-boxes of the external wheelset of front bogie. While the vehicle runs in the full-curve section, a mechanical failure of one journal in the trailing wheelset of the front bogie is simulated by suddenly setting to zero the force transmitted by the corresponding primary suspension. This leads to the derailment of the front bogie and then to the impact of the leading wheelset of the same bogie with the derailment containment wall. Since the aim of this paper is to analyse the interaction of the derailed vehicle with the DCW, the derailment phase of the vehicle is not reported here.

Focusing on the impact between the two systems, once the vehicle and the DCW come into contact the normal force is computed using Equation (9). The results of the simulation are reported in Fig. (3), where the normal force F_N (left) at the single impact point is plotted with respect to the abscissa x_w of the contact point in the DCW reference frame. The first impact occurs after 10 m as prescribed, in order to avoid unwanted boundary effects. The impact force suddenly grows after the impact, due to the high stiffness of the structure. After having been in contact with the DCW over approximately 2 m (x_w=10-12 m), the axle box looses contact with the wall and impacts again a few meters later, until this force settles on nearly constant value and the DCW acts as a

guide for the derailed vehicle to a relatively low and nearly constant value which is the centripetal force applied by the DCW to guide the derailed vehicle along the curve. Fig. (3) (right) instead shows the time-history of the integral of the bending moment calculated along the length of base of the DCW using Equation (13). As expected, the maximum value of the integral of the bending moment takes place immediately after the initial impact, and an oscillatory trend can be clearly seen as the structure itself starts oscillating.

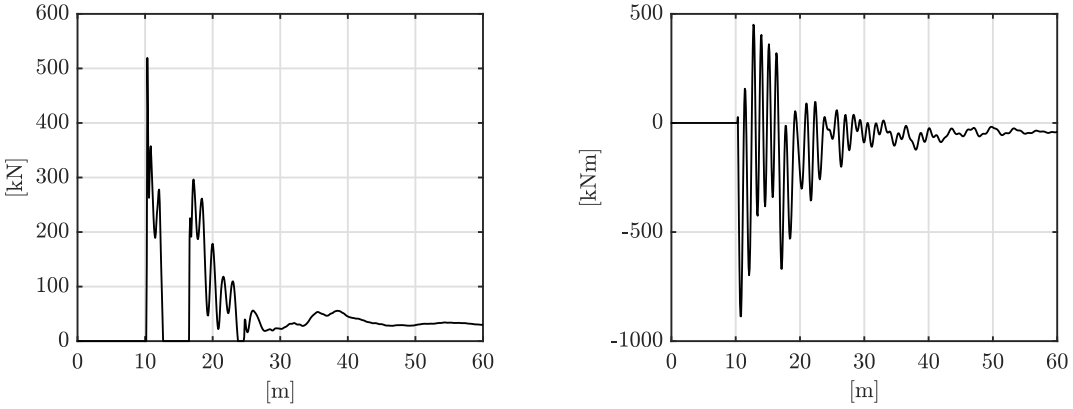

Figure 3: Left: Normal impact force between derailment containment wall and the derailed vehicle with respect of x_w of the structure. Right: Integral of the bending moment at the base of the derailment containment wall with respect of x_w of the structure. The first impact is 10 m after the starting point of the DCW.

In Fig. (4) (left), the distribution of the bending moment along the foundation of the DCW is shown, considering the time instant immediately after the impact, corresponding to x_w = 10 m. It is worth pointing out that the integral of this distribution over the total length of the structure (80 m) will lead to the peak value in Fig. (3) (right). Another important result, shown in this plot, is that the influence region of the first and maximum impact is $\pm$ 5 m approximately. Fig. (4) (right) shows the distribution of the bending moment across the entire wall surface, at a time instant closely following the first interaction of the wall with the derailed vehicle. As expected, the maximum bending moment takes place at the base of the structure, exactly under the impact point at 10 m.

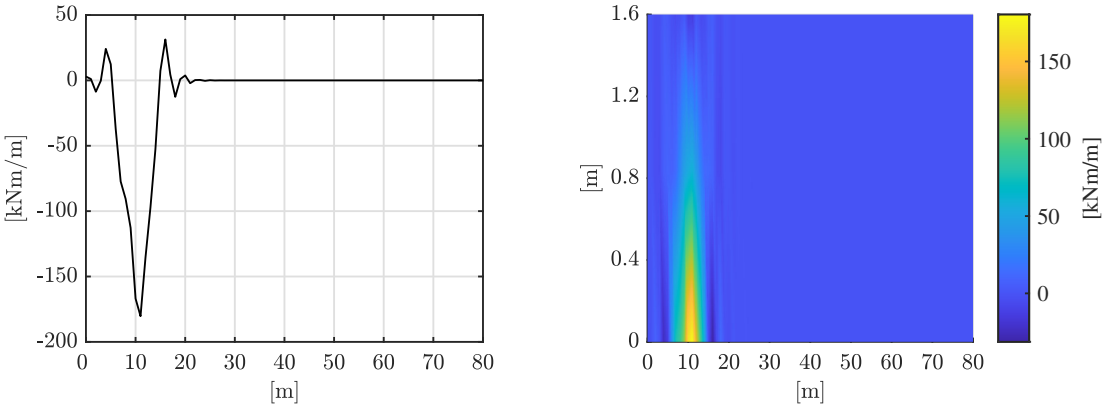

Figure 4: Left: Distribution of the bending moment at the base of the derailment containment wall along its total length (80 m) at the first impact with the derailed vehicle. Right: Distribution of the bending moment on the overall surface of the DCW (1.6 m x 80 m) at the same time.

Finally, a sensitivity analysis in terms of maximum impact force and bending moment is performed changing some parameters that define the dimensions and the position of the DCW with respect to track centre-line. Referring to Fig. (2), the parameters changed are the height of the wall h_w affecting the structure dimensions and as consequence the total mass, and the distance from the centre-line d. In configuration #0, considered as the reference case, the DCW is placed 2.2 m outside the track centreline an is 1.7 m tall. All the configurations analysed are shown in Table 1, where the results are also reported in terms of the parameters that define the tested scenario: peak impact forces, maximum bending moments at the foundation of the DCW and maximum moments for unit length. Focusing on the analysis related to the position of the DCW with respect to the track centreline, two different configurations (#1.a and #1.b) have been simulated by modifying the distance of DCW from the track by a $\pm$ 0.3 m amount. The results of the simulations are reported in Fig. (5). The left plot shows the trend of the integral of the bending moment at the base of the DCW (blue line) in case the DCW is closer to the centreline compared with the configuration #0 (dotted black line), while the right plot reports the same quantity but in case the DCW is farther from the centreline by 0.3 m, again compared with the simulation obtained with configuration #0. The differences are small since the wall is shifted by a small amount, but it can be seen that the closer the wall is to the track, the lower is the peak of the bending moment transmitted at the base of the structure, see also the peak values compared in Table 1. Conversely, the farther the wall is from the track, the higher the angle at which the vehicle impacts, resulting in a higher peak of bending moment. It should be remembered that these analyses do not take into account the fact that the vehicle, once derailed, must travel some distance on the ballast rocks and the sleepers, and this could affect the results obtained so far.

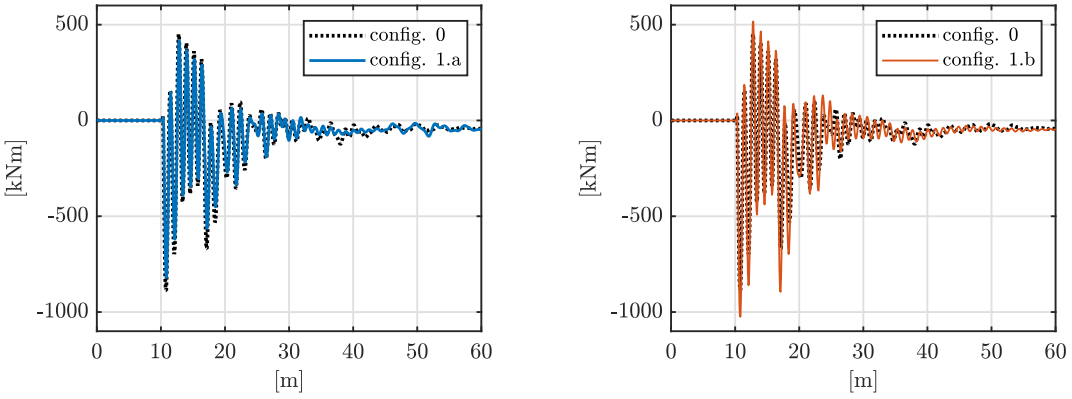

Figure 5: Integral of the bending moment at the base of the DCW with respect of x_w in case of distance from the centreline is - 0.3 m with respect of configuration 0 (left) or + 0.3 m (rigth).

As far as the sensitivity analysis on the dimensions of the structure is concerned a change of this parameter has influence on two aspects: it increases the height of impact point with respect of the base of the DCW (arm with which the force is transmitted to the base of the DCW) but also the total mass of the structure will be affected. The result is therefore influenced by the effect of these two changes in a combined way. By increasing the arm, the moment slightly increases but, at the same time, it is mitigated by the fact that the mass for unit length has also increased. A higher mass of the structure has an effect on the inertia force of the DCW that arise a the very beginning of the impact and reacts with the impulsive part of the contact, reducing the overall elastic bending moment at the foundations. Finally, two different scenarios (#2.a and #2.b) have been simulated: by increasing the height of DCW respectively by 0.25 m and 0.5 m. For the sake of brevity, only the peak values of the bending moment of these simulations are reported in Table 1.

Table 1: Results of the simulations of the different configurations in terms of peak impact force F, integral of the bending moment at the base of the DCW M and moment per unit length M^*.

#	h_{DCW}	D	F	M_{tot}	M^*
-	$[m]$	$[m]$	$[kN]$	$[kNm]$	$[kNm/m]$
0	1.65	2.2	435	886	181
1.a	1.65	1.9	385	820	175
1.b	1.65	2.4	528	1018	212
2.a	1.90	2.2	436	879	164
2.b	2.15	2.2	483	916	158

4 CONCLUSION

In this paper, a model that simulates the dynamics of a derailed train with focus on its subsequent interaction with a deformable containment structure is presented. The specific derailment case considered in the paper is due to the mechanical failure of one axle journal and causes the front bogie of the vehicle to collide with the flexible containment structure, modelled according to the finite element method using Kirchoff plate elements. Different positions and dimensions of the DCW have been considered and for each one of these the loads from the impact and the bending moment in the structure have been computed.

From the sensitivity analyses regarding the position and size (height) of the DCW, it has been shown that the distance from the centre line of the track has a greater influence than its height. Furthermore, the further the structure is from the track, the higher the bending moment at the base. Conversely, a closer structure will be subjected to a slightly lower bending moment. A change in the height of the wall does not produce significant variations in reaction forces on the structure. A detailed model of the interaction of the derailed wheels with the ballast and sleepers is targeted as the next development of the model. Finally, the aim of this research is to analyse different layouts of the DCW, in order to obtain results that can be used for the structural sizing of the structure itself.

ACKNOWLEDGMENTS

Financial support to this research from company Rete Ferroviaria Italinana – RFI under contract 175/21CR is gratefully acknowledged.

REFERENCES

[1] Liu, X., Saat, M.R., Barkan, C.P.L.: Analysis of causes of major train derailment and their effect on accident rates. Transportation Research Record **2289**(1) (2012) 154–163 doi:10.3141/2289-20.

[2] Wu, X., Chi, M., Gao, H.: Post-derailment dynamic behaviour of a high-speed train under earthquake excitations. Engineering Failure Analysis **64**(1) (2016) 97–110 doi:10.1016/j.engfailanal.2016.03.005.

[3] Diana, G., Sabbioni, E., Somaschini, C., Tarsitano, D., Cavicchi, P., Mario, M.D., Labbadia, L.: Full-scale derailment tests on freight wagons. Vehicle System Dynamics **60**(6) (2022) 1849–1866 doi:10.1080/00423114.2021.1877745.

[4] Braghin, F., Bruni, S., Diana, G.: Experimental and numerical investigation on the derailment of a railway wheelset with solid axle. Vehicle System Dynamics **44**(4) (2006) 305–325 doi:10.1080/00423110500337494.

[5] Brabie, D.: On the Influence of Rail Vehicle Parameters on the Derailment Process and its Consequences. PhD thesis, KTH, Aeronautical and Vehicle Engineering (2012) ISBN:91-7283-806-X.

[6] Robinson PM, Scott P, L.B., et al.: Development of the future rail freight system to reduce the occurrences and impact of derailment- d-rail - summary report and database of derailments incidents. EU D-RAIL project (2011)

[7] Hung, C., Suda, Y., Aki, M., Tsuji, T., Morikawa, M., Yamashita, T., Kawanabe, T., Kunimi, T.: Study on detection of the early signs of derailment for railway vehicles. Vehicle System Dynamics **48**(sup1) (2010) 451–466 doi:10.1080/00423114.2010.486862.

[8] Iwnicki, S.: Handbook of Railway Vehicle Dynamics. CRC Press, Boca Raton, USA (2006) doi:10.1201/9781420004892.

[9] Tanabe, M., Goto, K., Watanabe, T., Sogabe, M., Wakui, H., Tanabe, Y.: A simple and efficient numerical model for dynamic interaction of high speed train and railway structure including derailment during an earthquake. Procedia Engineering **199** (2017) 2729–2734 doi:10.1016/j.proeng.2017.09.298.

[10] Brabie, D., Andersson, E.: Post-derailment dynamic simulation of rail vehicles – methodology and applications. Vehicle System Dynamics **46**(sup1) (2008) 289–300 doi:10.1080/00423110801939162.

[11] Brabie, D., Andersson, E.: On minimizing derailment risks and consequences for passenger trains at higher speeds. Proceedings of the Institution of mechanical engineers. Part F, Journal of Rail and Rapid Transit **223**(6) (2009) 543–566 doi:10.1243/09544097JRRT271.

[12] Lai, J., Xu, J., Wang, P., Chen, J., Fang, J., Ma, D., Chen, R.: Numerical investigation on the dynamic behaviour of derailed railway vehicles protected by guard rail. Vehicle System Dynamics **59**(12) (2021) 1803–1824 doi:10.1080/00423114.2020.1792941.

[13] Bae, H.U., Yun, K.M., Lim, N.H.: Containment capacity and estimation of crashworthiness of derailment containment walls against high-speed trains. Proceedings of the Institution of Mechanical Engineers, Part F: Journal of Rail and Rapid Transit **232**(3) (2018) 680–696 doi:10.1177/0954409716684663.

[14] Song, I.H., Kim, J.W., Koo, J.S., Lim, N.H.: Modeling and simulation of collision-causing derailment to design the derailment containment provision using a simplified vehicle model. Applied Sciences **10**(1) (2020) doi:10.3390/app10010118.

[15] Shabana, A.A.: Dynamics of Multibody Systems. Cambridge University Press, Cambridge, UK (2020) doi:10.1017/9781108757553.

[16] Bruni, S., Vinolas, J., Berg, M., Polach, O., Stichel, S.: Modelling of suspension components in a rail vehicle dynamics context. Vehicle System Dynamics **49**(7) (2011) 1021–1072 doi:10.1080/00423114.2011.586430.

[17] Przemieniecki, J.S.: Theory of matrix structural analysis. McGraw-Hill Book Company, New York, USA (1968) ISBN:0486649482.

[18] Lankarani, H., Nikravesh, P.: A contact force model with hysteresis damping for impact analysis of multibody systems. Journal of Mechanical Design **112**(9) (1990) 369–376 doi:10.1115/1.2912617.

[19] Rao, S.S.: Vibration of Continuous Systems. John Wiley Sons Ltd, New York, USA (2006) doi:10.1002/9780470117866.